# A multiresolution triangular plate-bending element method

YiMing Xia
(Civil Engineering Department, Nanjing University of Aeronautics and Astronautics, Nanjing, P.R.China)
email:xym4603@sina.com

**Abstract**

A triangular plate-bending element with a new multi-resolution analysis (MRA) is proposed and a novel multiresolution element method is hence presented. The MRA framework is formulated out of a displacement subspace sequence whose basis functions are built out of scaling and shifting on the element domain of basic full node shape function. The basic full node shape function is constructed by means of extending the shape function triangle domain for a split node at the zero coordinates to the hexagon area enclosing the zero coordinates. As a result, a new split-full node notion is presented and a novel rational MRA concept together with the resolution level (RL) is constituted for the element. Via practical examples, it is found that the traditional triangular plate element and method is a mono-resolution one and also a special case of the proposed element and method. The meshing for the monoresolution plate element model is based on the empiricism while the RL adjusting for the multiresolution is laid on the rigorous mathematical basis. The analysis clarity of a plate structure is actually determined by the RL, not by the mesh. Thus, the accuracy of a structural analysis is replaced by the clarity, the irrational MRA by the rational and the mesh model by the RL that is the discretized model by the integrated. The continuous full node shape function unveils secrets behind assembling artificially of node-related items in global matrix formation by the conventional FEM.

**Keywords:** Triangular Plate-bending Element; Split Node; Full Node; Analysis Clarity; Displacement Subspace Sequence; Rational Multiresolution Analysis; Resolution Level

## 1. Introduction

Multi-resolution analysis (MRA) is a popular technique that has been applied in many domains such as the signal and image processing, the damage detection and health monitoring, the differential equation solution, etc. However, in the field of computational mechanics, the MRA has not been, in a real sense, fully utilized in the numerical solution of engineering problems either by the traditional finite element method (FEM)[1] or by other methods such as the wavelet finite element method (WFEM)[2, 3], the meshfree method (MFM)[4, 5], the natural element method (NEM)[6, 7] and isogeometric analysis method (IGAM) [8, 9],etc.

As is commonly known of the FEM, owing to the invariance of node number a single finite element contains, the finite element can be regarded as a monoresolution one from a MRA point of view and the FEM structural analysis is usually not associated with the MRA concept. The MRA seems to be rarely used when the FEM is employed to numerical analysis. However, it is, in fact, by means of meshing and re-meshing in which a cluster of monoresolution finite elements with each split nodes are assembled together artificially that the rough MRA is executed by the FEM. As we can see, in overall analysis process of a structure by the FEM, there is no mathematical foundation for the traditional finite element meshing and the finite elements are assembled together artificially. The traditional finite element model has to be re-meshed until sufficient accuracy is reached, which leads to the low computation efficiency or convergent rate. The deficiency of the FEM becomes much explicit in the accurate computation of structural problems with local steep gradient such as material nonlinear [10, 11], local damage and crack [12, 13], impacting and exploding problems [14, 15].

The great efforts have been made over the past thirty years to overcome the drawbacks of the FEM with many improved methods to come up, such as WFEM, IGAM, MFM and NEM etc, which open up a transition from the monoresolution finite element method to the multiresolution finite element method featured with an integrated element model. Although these MRA methods have illustrated their powerful capability and computational efficiency in dealing with some problems, they always have such major inherent deficiencies as the complexity of full node shape function construction by tensor-product or polynomial coefficient numerical simulating technique, the absence of the Kronecker property and the lack of a rigorous mathematical basis for the MRA, which make the treatment of element boundary condition complicated and the selection of element node layout empirical, that substantially reduce computational efficiency. Hence, these MRA methods have never found a wide application in engineering practice just as the FEM. In fact, they can be viewed as the intermediate products in the transition of the FEM from the monoresolution to the multiresolution.

The deficiencies of all those MRA methods can be eliminated by the introduction of a new multiresolution element method in this paper. With respect to the plate element in the finite element stock, a new multiresolution triangular plate-bending element is formulated by a new MRA, which is constituted by scaled and translated version as subspace basis functions of the basic full node shape functions. The basic full node shape functions are then constructed from making a series of parallelograms to superimpose identical triangle-defined domains for split nodes around the origin of coordinates. Hence, the full node shape function construction is quite simple and clear. In addition, the proposed element method possesses a simple, clear and rigorous mathematical basis for MRA, which endows the proposed element with the resolution level (RL) that can be modulated to freely change the node number and position in the element, adjusting structural analysis accuracy accordingly. As a result, the proposed element method can bring about substantial improvement of the computational efficiency in the structural analysis when compared with the corresponding FEM or other MRA methods.

## 2. Basic full node shape function

As shown in Fig.1*a.b*, an arbitrary triangle plate element is set against a Carstesian coordinate system with the geometric configuration of the bottom sideline length as $a$, the height as $h$. Obviously, The analytical functions for the bottom sideline in the coordinate system can be written in dimensionless quantity as

$$\frac{y}{h}=0 \tag{1}$$

For the other sideline (not one that goes through the coordinate origin) is assumed as

$$\frac{x}{a}+\frac{y}{b}=1 \tag{2}$$

Where *a*,*b* are denoted as the horizontal and the vertical intercepts respectively.
For the third is determined as

$$\frac{x}{a}-\left(\frac{1}{h}-\frac{1}{b}\right)y=0 \quad (b\geq h) \tag{3}$$

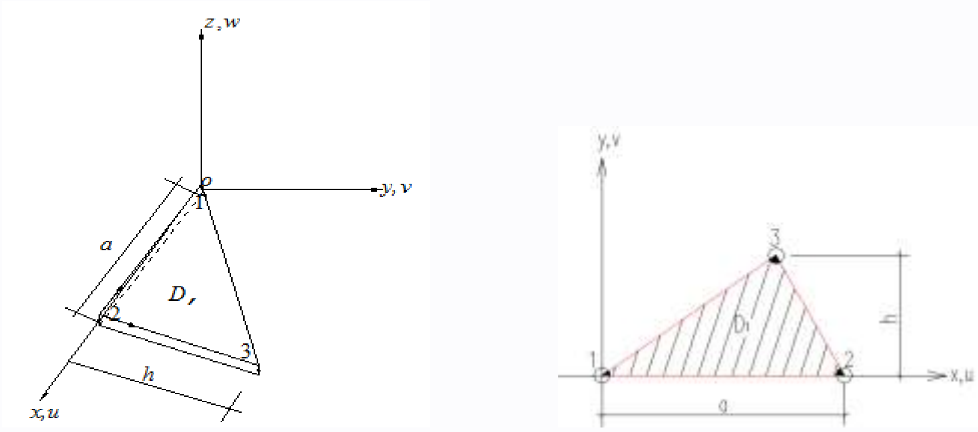


***a.*** A triangular plate ***b.*** The mid-plane of the plate

**Fig 1.** A triangular plate-bending element

Afterward, the transverse displacement $w^e$ in *z* axis direction at an arbitrary point within the triangular plate element can be defined as

$$w^e=\sum_{i=1}^{3}N_i w_i+\sum_{i=1}^{3}N_{xi}\theta_{xi}+\sum_{i=1}^{3}N_{yi}\theta_{yi} \tag{4}$$

where $w_i, \theta_{xi}, \theta_{yi}$ are the transverse, rotational displacements at node *i* of the element respectively in the Carstesian coordinate system. $N_i$ , $N_{xi}$ , $N_{yi}$ are the conventional shape functions at the node *i* ( *i* =1,2,3)，which are defined on the domain $D_1$ as follows

$$N_1=L_1+L_1^2L_2+L_1^2L_3-L_1L_2^2-L_1L_3^2$$

$$N_{x1}=-b_3\left(L_1^2L_2+\frac{1}{2}L_1L_2L_3\right)+b_2\left(L_3L_1^2+\frac{1}{2}L_1L_2L_3\right)$$

$$N_{y1}=-c_3\left(L_1^2L_2+\frac{1}{2}L_1L_2L_3\right)+c_2\left(L_3L_1^2+\frac{1}{2}L_1L_2L_3\right)$$

$$b_3=y_1-y_2,\quad c_3=x_2-x_1,\quad b_2=y_3-y_1,\quad c_2=x_1-x_3$$

Based on the analytical functions for the three triangle sidelines obtained above, the following relationship can be gotten:

$$L_1 = 1 - \left(\frac{x}{a} + \frac{y}{b}\right), \quad L_2 = \frac{x}{a} - \left(\frac{1}{h} - \frac{1}{b}\right) y, \quad L_3 = \frac{y}{h}, \quad x, y \in D_1 \tag{5a,b,c}$$

Obviously, there exists relationship $L_1 + L_2 + L_3 = 1$

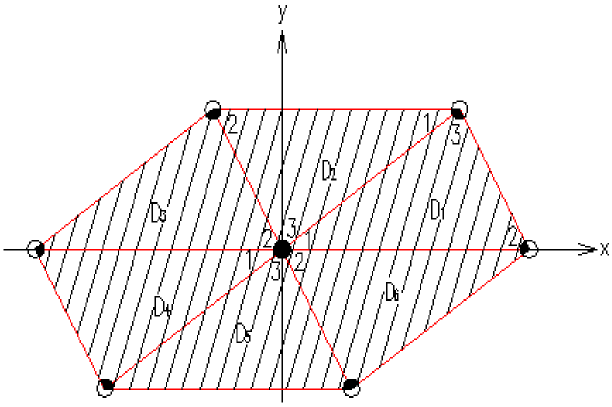


**Fig 2.** The extended hexagon domain enclosing a node at the coordinate origin

As we can see in Fig.1*b*, the supporting domain (shaded area $D_1$) of the triangular element contains only a part (blackened portion) of a full node, that means a full node is broken up into split nodes in the process of the traditional node shape function construction and all full nodes within the structural domain are thus discretized by meshing. In order to formulate a full node shape function or constitute an integrated computational model, the single triangle-defined domain for the split node should be extended to the hexagon area by means of successively building up a series of parallelograms to superimpose identical triangle-defined regimes around the coordinate origin. Subsequently, the node at the coordinate zero is enclosed by the hexagon domain (shaded area) as shown in Fig.2. The basic shape function for the full node (blackened node) at the coordinate origin can be defined as following:

$$\phi(x,y) = \begin{cases} N_1(x,y) & (x, y \in D_1) \\ N_3(x,y) & (x, y \in D_2) \\ N_2(x,y) & (x, y \in D_3) \\ N_1(x,y) & (x, y \in D_4) \\ N_3(x,y) & (x, y \in D_5) \\ N_2(x,y) & (x, y \in D_6) \end{cases} \tag{6}$$

$$\phi_x(x,y) = \begin{cases} N_{x1}(x,y) & (x, y \in D_1) \\ N_{x3}(x,y) & (x, y \in D_2) \\ N_{x2}(x,y) & (x, y \in D_3) \\ N_{x1}(x,y) & (x, y \in D_4) \\ N_{x3}(x,y) & (x, y \in D_5) \\ N_{x2}(x,y) & (x, y \in D_6) \end{cases} \tag{7}$$

$$\phi_y(x,y)=\begin{cases} N_{y1}(x,y) & (x,y\in D_1) \\ N_{y3}(x,y) & (x,y\in D_2) \\ N_{y2}(x,y) & (x,y\in D_3) \\ N_{y1}(x,y) & (x,y\in D_4) \\ N_{y3}(x,y) & (x,y\in D_5) \\ N_{y2}(x,y) & (x,y\in D_6) \end{cases} \qquad (8)$$

where $N_i$ , $N_{xi}$ , $N_{yi}$ are the shape functions at the node $i$ ( $i$ =1,2,3), which are defined on the domains of $D_1$, $D_2$ , $D_3$ , $D_4$ , $D_5$ , $D_6$ corresponding to six split nodes around the coordinate origin respectively.

In light of the regular node shape function construction method by area coordinates for a triangular plate element, the six split node shape functions can be founded by the analytical functions for the six sidelines of the hexagon in the Carstesian coordinate system. Based on the analytical functions for three triangular sidelines (1), (2), (3), the three upper hexagon sideline functions are easily written as

$$\frac{x}{a}+\frac{y}{b}=1 \qquad (9a)$$

$$\left(\frac{1}{h}-\frac{1}{b}\right)y-\frac{x}{a}=1 \qquad (9b)$$

$$\frac{y}{h}=1 \quad , \qquad (9c)$$

Therefore, the three lower hexagon sideline function expressions can be easily obtained by shifting each upper sideline a distance along *x*,*y* axis respectively, that is

$$\frac{x}{a}+\frac{y}{b}=-1 \qquad (10a)$$

$$\left(\frac{1}{h}-\frac{1}{b}\right)y-\frac{x}{a}=-1 \qquad (10b)$$

$$\frac{y}{h}=-1 \quad , \qquad (10c)$$

As a result, based on the hexagon sideline analytical functions, the split node shape functions on the domains of $D_2$ , $D_3$ , $D_4$ , $D_5$ , $D_6$ can be founded respectively as

$$\begin{cases} L_1=\frac{x}{a}+\frac{y}{b}, \quad L_2=\left(\frac{1}{h}-\frac{1}{b}\right)y-\frac{x}{a}, \quad L_3=1-\frac{y}{h}, \quad x,y\in D_2 \\ N_3=L_3+L_3^2L_1+L_3^2L_2-L_3L_1^2-L_3L_2^2 \\ N_{x3}=-b_2\left(L_3^2L_1+\frac{1}{2}L_1L_2L_3\right)+b_1\left(L_2L_3^2+\frac{1}{2}L_1L_2L_3\right) \end{cases}$$

$$\begin{cases} N_{y3} = -c_2\left(L_3^2L_1 + \dfrac{1}{2}L_1L_2L_3\right) + c_1\left(L_2L_3^2 + \dfrac{1}{2}L_1L_2L_3\right) \\ b_2 = y_3 - y_1, \quad c_2 = x_1 - x_2, \quad b_1 = y_2 - y_3, \quad c_1 = x_3 - x_2 \end{cases}$$

$$\begin{cases} L_1 = -\left(\dfrac{x}{a} + \dfrac{y}{b}\right), \quad L_2 = 1 - \left(\dfrac{1}{h} - \dfrac{1}{b}\right)y + \dfrac{x}{a}, \quad L_3 = \dfrac{y}{h}, \ x, y \in D_3 \\ N_2 = L_2 + L_2^2L_3 + L_2^2L_1 - L_2L_3^2 - L_2L_1^2 \\ N_{x2} = -b_1\left(L_2^2L_3 + \dfrac{1}{2}L_1L_2L_3\right) + b_3\left(L_1L_2^2 + \dfrac{1}{2}L_1L_2L_3\right) \\ N_{y2} = -c_1\left(L_2^2L_3 + \dfrac{1}{2}L_1L_2L_3\right) + c_3\left(L_1L_2^2 + \dfrac{1}{2}L_1L_2L_3\right) \\ b_1 = y_2 - y_3, \quad c_1 = x_3 - x_2, \quad b_3 = y_1 - y_2, \quad c_3 = x_2 - x_1 \end{cases}$$

$$\begin{cases} L_1 = 1 + \dfrac{x}{a} + \dfrac{y}{b}, \quad L_2 = \left(\dfrac{1}{h} - \dfrac{1}{b}\right)y - \dfrac{x}{a}, \quad L_3 = -\dfrac{y}{h}, \ x, y \in D_4 \\ N_1 = L_1 + L_1^2L_2 + L_1^2L_3 - L_1L_2^2 - L_1L_3^2 \\ N_{x1} = -b_3\left(L_1^2L_2 + \dfrac{1}{2}L_1L_2L_3\right) + b_2\left(L_3L_1^2 + \dfrac{1}{2}L_1L_2L_3\right) \\ N_{y1} = -c_3\left(L_1^2L_2 + \dfrac{1}{2}L_1L_2L_3\right) + c_2\left(L_3L_1^2 + \dfrac{1}{2}L_1L_2L_3\right) \\ b_3 = y_1 - y_2, \quad c_3 = x_2 - x_1, \quad b_2 = y_3 - y_1, \quad c_2 = x_1 - x_3 \end{cases}$$

$$\begin{cases} L_1 = -\left(\dfrac{x}{a} + \dfrac{y}{b}\right), \quad L_2 = \dfrac{x}{a} - \left(\dfrac{1}{h} - \dfrac{1}{b}\right)y, \quad L_3 = 1 + \dfrac{y}{h}, \ x, y \in D_5 \\ N_3 = L_3 + L_3^2L_1 + L_3^2L_2 - L_3L_1^2 - L_3L_2^2 \\ N_{x3} = -b_2\left(L_3^2L_1 + \dfrac{1}{2}L_1L_2L_3\right) + b_1\left(L_2L_3^2 + \dfrac{1}{2}L_1L_2L_3\right) \\ N_{y3} = -c_2\left(L_3^2L_1 + \dfrac{1}{2}L_1L_2L_3\right) + c_1\left(L_2L_3^2 + \dfrac{1}{2}L_1L_2L_3\right) \\ b_2 = y_3 - y_1, \quad c_2 = x_1 - x_2, \quad b_1 = y_2 - y_3, \quad c_1 = x_3 - x_2 \end{cases}$$

$$\begin{cases} L_1 = \dfrac{x}{a} + \dfrac{y}{b}, \quad L_2 = 1 - \dfrac{x}{a} + \left(\dfrac{1}{h} - \dfrac{1}{b}\right)y, \quad L_3 = -\dfrac{y}{h}, \ x, y \in D_6 \\ N_2 = L_2 + L_2^2L_3 + L_2^2L_1 - L_2L_3^2 - L_2L_1^2 \\ N_{x2} = -b_1\left(L_2^2L_3 + \dfrac{1}{2}L_1L_2L_3\right) + b_3\left(L_1L_2^2 + \dfrac{1}{2}L_1L_2L_3\right) \\ N_{y2} = -c_1\left(L_2^2L_3 + \dfrac{1}{2}L_1L_2L_3\right) + c_3\left(L_1L_2^2 + \dfrac{1}{2}L_1L_2L_3\right) \\ b_1 = y_2 - y_3, \quad c_1 = x_3 - x_2, \quad b_3 = y_1 - y_2, \quad c_3 = x_2 - x_1 \end{cases}$$

in which there exist relationships $1 \ge L_1 \ge 0$, $1 \ge L_2 \ge 0$, $1 \ge L_3 \ge 0$, $L_1 + L_2 + L_3 = 1$ in the various domains of $D_2$, $D_3$, $D_4$, $D_5$, $D_6$ respectively.

Up to now, the basic full node shape functions $\phi(x,y), \phi_x(x,y), \phi_y(x,y)$ for the triangular plate-bending element can be graphed respectively in Fig.3.

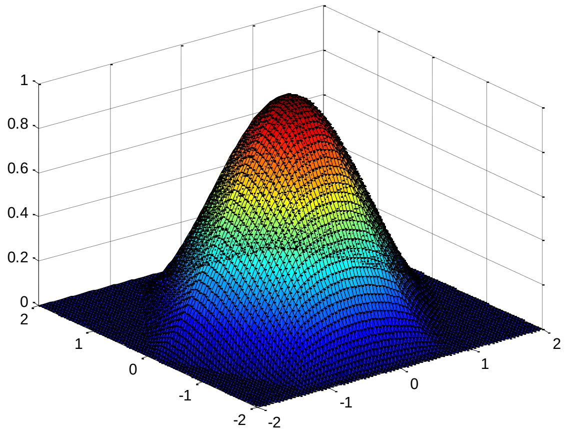


***a.*** $\phi(x,y)$

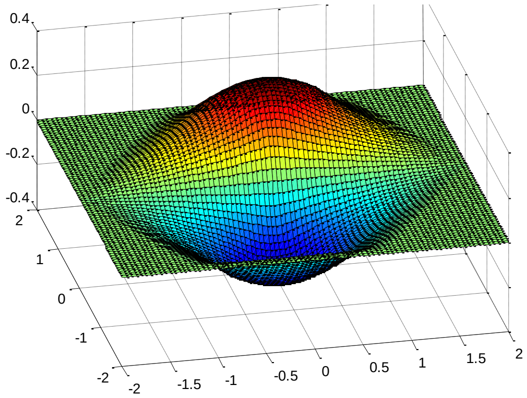


***b.*** $\phi_x(x,y)$

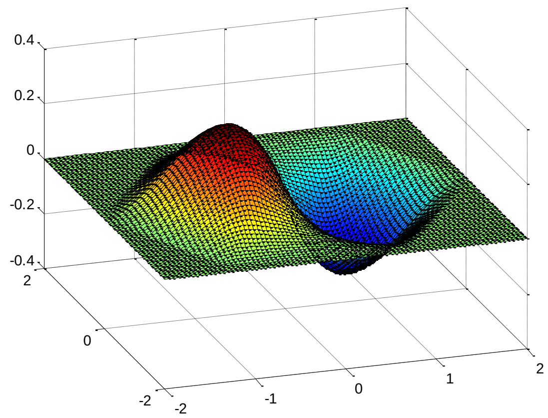


***c.*** $\phi_y(x,y)$

**Fig.3.**The basic full node shape functions $\phi(x,y), \phi_x(x,y), \phi_y(x,y)$ at the coordinate origin

It is evident that the basic full node shape functions $\phi(x,y), \phi_x(x,y), \phi_y(x,y)$ are continuous and possess the Kronecker delta property as follows：

$$\begin{cases} \phi(0,0)=1 \quad \phi(6points)=0 \quad \dfrac{\partial\phi(0,0)}{\partial x}=0 \\ \dfrac{\partial\phi(0,0)}{\partial y}=0 \quad \dfrac{\partial\phi(6points)}{\partial x}=0 \quad \dfrac{\partial\phi(6points)}{\partial y}=0 \\ \phi_x(0,0)=0 \quad \phi_x(6points)=0 \quad \dfrac{\partial\phi_x(0,0)}{\partial x}=0 \\ \dfrac{\partial\phi_x(0,0)}{\partial y}=1 \quad \dfrac{\partial\phi_x(6points)}{\partial x}=0 \quad \dfrac{\partial\phi_x(6points)}{\partial y}=0 \\ \phi_y(0,0)=0 \quad \phi_y(6points)=0 \quad \dfrac{\partial\phi_y(0,0)}{\partial x}=-1 \\ \dfrac{\partial\phi_y(0,0)}{\partial y}=0 \quad \dfrac{\partial\phi_y(6points)}{\partial x}=0 \quad \dfrac{\partial\phi_y(6points)}{\partial y}=0 \end{cases} \tag{11}$$

## 3. Displacement Subspace Sequence

In order to carry out a MRA of a thin plate structure, the mutual nesting displacement subspace sequence for a plate element should be established. In this paper, a totally new technique is proposed to construct the MRA which is based on the concept that a subspace sequence (multi-resolution subspaces) can be formulated by subspace basis function vectors at different resolution levels whose elements-scaling function vector can be constructed by scaling and shifting on the domain of the basic full node shape functions. As a result, the displacement subspace basis function vector at an arbitrary resolution level (RL) of $\frac{1}{2}(m+1)\times(m+2)$ for a triangular membrane element is formulated as follows:

$$\mathbf{\Psi}_m=\left[\mathbf{\Phi}_{mm,00}\cdots\mathbf{\Phi}_{mm,rs}\cdots\mathbf{\Phi}_{mm,mm}\right] \tag{12}$$

where $\mathbf{\Phi}_{mn,rs}=\left[\phi_{mm,rs} \quad \phi_{xmm,rs}/m \quad \phi_{ymm,rs}/m\right]$ is the scaling basis function vector, $\phi_{mm,rs}=\phi(mx-r,my-s)$ , $\phi_{xmm,rs}=\phi_x(mx-r,my-s)$ , $\phi_{ymm,rs}=\phi_y(mx-r,my-s)$ , $m$ denoted as the positive integers, the scaling parameters in $x$ ,$y$ directions respectively. $r$, $s$ as the positive integers, the node position parameters, that is $r=0,1,2,3\cdots m$, $s=0,1,2,3\cdots m$, Here, $(mx-r)\in[-a,a]$ $(my-s)\in[-h,h]$, $x,y\in D_1$ .

It is seen from Eq. (11) that the nodes for the scaling process are equally spaced on the triangle domain $D_1$ in $x$ ,$y$ directions respectively

Scaling of the basic full node shape function and then shifting to other nodes $\left(\frac{a}{m}\left(r-s\frac{h}{b}\right),\frac{s}{m}h\right)$ within the element domain $D_1$ $(m\geq r\geq s)$ will produce the various full node shape functions.

Since the elements in the base functions are linearly independent with the various scaling and the different shifting parameters, the subspaces in the subspace sequence can be established, thus formulating a MRA framework, that is

$$\mathbf{W}_m = [V_1 \ldots \quad V_i \ldots . \quad V_m] \tag{13a}$$

$$V_i := span\{\mathbf{\Psi}_i : i \in Z\} \tag{13b}$$

If $I = 2i$, then $V_i \subset V_I$ (13c)

Thus, it can be found that the displacement subspace sequence $\mathbf{W}_m$ can be taken for a solid mathematical foundation for the MRA framework and $V_1$ is equivalent to the displacement field for a traditional 3-node plane triangular element that is the reason why the traditional triangular plate element is regarded as a mono-resolution one and also a special case of the multiresolution triangular.

Based the MRA established, the deflection of the triangular plate element in the displacement subspace at RL of $\frac{1}{2}(m+1)\times(m+2)$ can be defined as follows

$$w_m^e = \mathbf{\Psi}_m \mathbf{a}_m^e \tag{14}$$

where $\mathbf{a}_{mn}^e = \left[[w_{00}, \theta_{x00}, \theta_{y00}] \ldots \quad [w_{rs}, \theta_{xrs}, \theta_{yrs}] \ldots \quad [w_{mn}, \theta_{xmn}, \theta_{ymn}]\right]^T$, $w_{rs}, \theta_{xrs}, \theta_{yrs}$ are the transverse and rotational displacements respectively at the element node $\left(\frac{a}{m}\left(r - s\frac{h}{b}\right), \frac{s}{m}h\right)$.

It is obvious that the proposed multi-resolution element is a meshfree one whose nodes are uniformly scattered, node number and position fully determined by the *RL*. When the scaling parameter m=1(*RL*=$\frac{1}{2}(2)\times(3) = 1\times 3$), that is a traditional 3-node triangular plate element, eq. (14) will be reduced to eq. (4).

## 4 Multiresolution triangular plate element

The generalized function of potential energy in a displacement subspace at the resolution level of $\frac{1}{2}(m+1)\times(m+2)$ for a triangular plate element can be defined as

$$\Pi(V_m) = \frac{1}{2}\iint_{D_1} [\kappa]_m^T [D_b][\kappa]_m \, dxdy - \iint_{D_1} q w_m^e dxdy - \sum_i Q_i w_{mi}^e \tag{15}$$

where $[\kappa]_m = -\begin{bmatrix} \frac{\partial^2 w_m^e}{\partial x^2} \\ \frac{\partial^2 w_m^e}{\partial y^2} \\ 2\frac{\partial^2 w_m^e}{\partial x \partial y} \end{bmatrix}$, $[D_b] = C_b \begin{bmatrix} 1 & \mu & 0 \\ \mu & 1 & 0 \\ 0 & 0 & (1-\mu)/2 \end{bmatrix}$, $C_b = \frac{Et^3}{12(1-\mu^2)}$, $E$ is the material Young modulus, $t$ the thickness of the element, $\mu$ the Poisson's ratio, $q$ distributed transverse loadings, $Q$ the lump transverse loadings. elastic modulus.

$$[\kappa]_m = [B_{00}, \cdots B_{rs}, \cdots B_{mm}]\mathbf{a}_m^e \tag{16}$$

where

$$B_{rs} = -\begin{bmatrix} \frac{\partial^2 \phi_{rs,m}}{\partial x^2} & \frac{\partial^2 \phi_{xrs,m}}{\partial x^2} & \frac{\partial^2 \phi_{yrs,m}}{\partial x^2} \\ \frac{\partial^2 \phi_{rs,m}}{\partial y^2} & \frac{\partial^2 \phi_{xrs,m}}{\partial y^2} & \frac{\partial^2 \phi_{yrs,m}}{\partial y^2} \\ 2\frac{\partial^2 \phi_{rs,m}}{\partial x \partial y} & 2\frac{\partial^2 \phi_{xrs,m}}{\partial x \partial y} & 2\frac{\partial^2 \phi_{yrs,m}}{\partial x \partial y} \end{bmatrix}$$

Substituting (13) into (14) and consolidating, we get

$$\Pi_p(V_m) = \frac{1}{2}\mathbf{a}_m^{eT}\mathbf{K}_m^e\mathbf{a}_m^e - \mathbf{a}_m^{eT}\mathbf{f}_m^e - \mathbf{a}_m^{eT}\mathbf{F}_m^e \tag{17}$$

in which $\mathbf{K}_m^e$ is denoted as the element stiffness matrix; $\mathbf{f}_m^e$ as the element distributed equivalent node force vector; $\mathbf{F}_m^e$ as the element concentrated equivalent node force vector.

According to the principal of minimums potential energy $\delta\Pi_p(V_m) = 0$, the following element equilibrium equations can be obtained

$$\mathbf{K}_m^e\mathbf{a}_m^e = \mathbf{f}_m^e + \mathbf{F}_m^e$$

where $\mathbf{K}_m^e = \begin{bmatrix} \mathbf{k}_{00}^{00} \cdots & \mathbf{k}_{rs}^{00} \cdots & \mathbf{k}_{mm}^{00} \\ \cdot & \cdot & \cdot \\ \cdot & \cdot & \cdot \\ \cdot & \cdot & \cdot \\ \mathbf{k}_{00}^{rs} \cdots & \mathbf{k}_{rs}^{rs} \cdots & \mathbf{k}_{ij}^{rs} \\ \cdot & \cdot & \cdot \\ \cdot & \cdot & \cdot \\ \cdot & \cdot & \cdot \\ \mathbf{k}_{00}^{mm} \cdot & \mathbf{k}_{rs}^{mm} \cdot & \mathbf{k}_{mm}^{mm} \end{bmatrix}$

in which the superscript denoted as the row number of the matrix and the subscript as the aligned element node numbering (*r*, *s*). In terms of the properties of the extended shape functions, we have

$$\begin{cases} \mathbf{k}_{rs}^{rs} = \sum\limits_{\substack{|c-r|\le 1 \\ |d-s|\le 1}} \mathbf{k}_{cd,rs} \\ \mathbf{k}_{rs}^{rs} = \mathbf{k}_{cd,rs} = 0, when |c-r| > 1, |d-s| > 1 \end{cases} \tag{18}$$

in which $\mathbf{k}_{cd,rs}$ is the coupled node stiffness matrix relating the node (*c*, *d*) to (*r*, *s*).

$$\mathbf{k}_{cd,rs} = \iint\limits_{D_1} \mathbf{B}_{cd}\mathbf{E}\mathbf{B}_{rs}^b dxdy \tag{19}$$

$$\begin{cases} \mathbf{f}_{m,rs}^{er} = \iint \left[\mathbf{\Phi}_{mm,rs}\right]^T qdxdy \\ \mathbf{F}_{m,rs}^{er} = \sum\limits_i \left[\mathbf{\Phi}_{mm,rs}\left(mx_i - r, my_i - s\right)\right]^T P_i \end{cases} \tag{20}$$

where $x_i$, $y_i$ is the local coordinate at the locations the lump loading acting on.

## 5.Transformation Matrix

In order to carry out structural analysis, the element stiffness and mass matrices $\mathbf{K}_m^e$ the loading column vectors $\mathbf{f}_m^e, \mathbf{F}_m^e$ should be transformed from the element local coordinate system (*xoy*) to the structural global coordinate system (*XOY*). The transforming relations from the local to the global are defined as follows:

$$\mathbf{K}_m^i = \mathbf{T}_m^{e\,T}\mathbf{K}_m^e\mathbf{T} \tag{21}$$

$$\mathbf{f}_m^i = \mathbf{T}_m^{eT}\mathbf{f}_m^e \tag{22}$$

$$\mathbf{F}_m^i = \mathbf{T}_m^{eT}\mathbf{F}_m^e \tag{23}$$

where $\mathbf{K}_m^i$ is the element stiffness matrix, $\mathbf{f}_m^i, \mathbf{F}_m^i$ the element loading column vectors under the global coordinate system. $\mathbf{T}_m^e$ is the element transformation matrix defined as follows;

$$\mathbf{T}_m^e = \begin{bmatrix} \boldsymbol{\lambda}_{11} & & & & \mathbf{0} \\ & \cdots & & & \\ & & \boldsymbol{\lambda}_{ij} & & \\ & & & \cdots & \\ \mathbf{0} & & & & \boldsymbol{\lambda}_{mm} \end{bmatrix}$$

The structural global stiffness, mass matrix $\mathbf{K}_m$, the global loading column vectors $\mathbf{f}_m$, $\mathbf{F}_m$ can be obtained by splicing

# 6. Numerical Example and Discussion

## 6.1 Numerical Example

**Example 1.** As shown in Fig.4, a two opposite edge simply supported and other two free $60^0$ skew plate with the geometric configuration of length $L$ and the Poisson's ratio $\mu = 0.3$ is subjected to the uniform transverse loading of magnitude $q$. Evaluate the deflection at the center point of the plate.

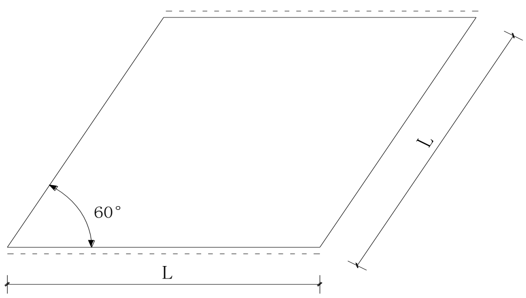


**Fig. 4.** A skew plate

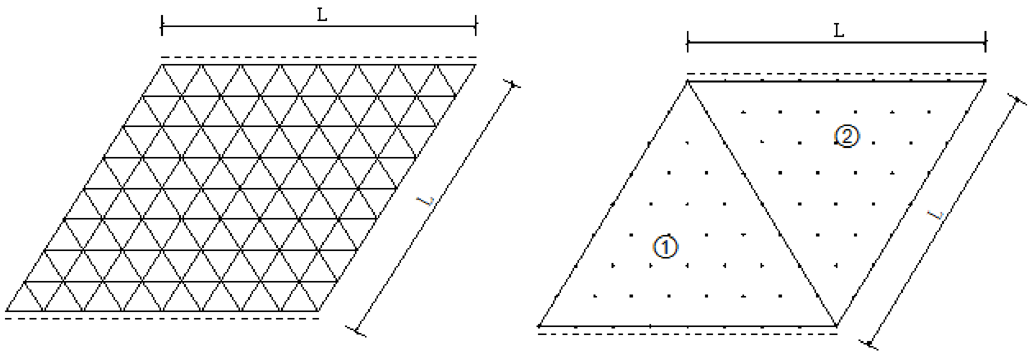


**(*a*)** The monoresolution discretized model **(*b*)** The multiresolution integrated model

**Fig. 5** The computational model for the skew plate

**Table.1**. the center point deflection for the skew plate($w$= β $\times qL^4$ /100$C_{\text{b}}$ )

| Element type | | |
|---|---|---|
| The proposed RL/RL/elem | The conventional (mesh) | Deflection( β ) |
| 9×9/5×9 | 8×8 | 0.7781 |
| 13×13/7×13 | 12×12 | 0.7863 |
| 17×17/9×17 | 16×16 | 0.7894 |
| One BSWI [3] | 0.7925 | |
| Analytical [16] | 0.7945 | |

The problem is usually tackled with regular meshes typified by a discretized model (split node) shown in Fig.5(*a*) These meshes are built of two-triangle rectangular mesh units and identified as $N_x \times N_y$, which denote the number of subdivisions in the $x$ and the $y$ dimensions. The solution can also be found by the multiresolution triangular-bending elements typified by an integrated model (full node) shown in Fig.5(*b*). These nodes are uniformly scattered in the two multiresolution triangular elements ①,② denoted by the RL, which represents the density of node uniform distribution. In the analysis process, these two multiresolution elements are spliced together along the common intersection boundary and the analysis clarity can be modulated by means of adjusting the RL. In addition, the wavelet model (full node) is made up of one 2D BSWI (B-spline wavelet on the interval) element of the jth scale=3, the mth order =4 are also employed abbreviated as BSWI43 with the DOF of 11×11. The results are summarized in the table1.It can be seen that the conventional and the proposed element methods exhibit identical monotonic increasing convergence to the 'exact' value with consistent mesh refinement and corresponding RL adjustment respectively.

Although the BSWI43 is of high accuracy, when compared with the proposed, the deficiencies of the BSWI element are obvious as follows. In light of tensor product formulation of the multidimensional MRA framework, the DOF of a multi-dimensional BSWI element will be so drastically increased from that of a one-dimensional element in an irrational way, resulting in complex full node shape functions and substantial reduction of the computational efficiency. Secondly, due to the absence of Kronecker delta property of the tensor-product constructed shape functions, the special treatments should be taken to deal with the element boundary condition, which will bring about low computational efficiency. Thirdly, there exists no such a parameter as the RL with a clear mathematical sense. With respect to the proposed and the conventional, the RL adjusting is more rationally and efficiently to be implemented than the meshing and the re-meshing for the following two reasons. Firstly, the RL adjusting is based on the MRA framework that is constructed on a solid mathematical basis while the meshing or remeshing, which resorts to the empiricism, has no MRA framework. Secondly, the stiffness matrix and the loading column vectors of the proposed element can be obtained automatically around the nodes while those of the traditional 3-node triangular plate-bending elements obtained by the artificially complex reassembling around the elements. Thus, the computational efficiency of the proposed element method is higher than the traditional one. In this way, the proposed plate element exhibits its strong capability of accuracy adjustment and its high power of resolution to identify details (nodes) of deformed structure by means of modulating its resolution level, just as a multiresolution camera with a pixel in its taken photo as a node in the proposed element. There appears no mesh in the proposed element just as no grid in a photo. Thus, an element of superior analysis accuracy surely has more nodes when compared with that of the inferior just as a clearer photo contains more pixels.

### 6.2 Discussion

Multiresolution analysis (MRA) can be viewed as a technique by which amount of element details that are exposed can be modulated at a request. The process of differential equation solution can be seen as one of structure node (detail) exposition. In the numerical analysis field, the node number a large-sized element contains could be adjusted respectively in various manners by different methods. Those approaches can be classified into two categories，one is the discretized model method, featured with split node shape functions, such as the traditional FEM, the multigrid FEM, the adaptive refinement FEM, etc., another is the integrated model approach, characterized by full node shape functions, such as the wavelet FEM (WFEM), the traditional meshfree method (MFM), the traditional natural element method (NEM), isogeometric analysis method (IGAM) and the proposed multiresolution element method (MEM) etc. FEM applies the scheme of meshing and re-meshing, which is mainly relied on the empiricism, to adjust the element node number in a rough way, thus performing an irrational MRA; WFEM adopts the technique of cubic B-spline function tensor product to form the full node shape functions that are complicated to be numerically integrated and to be utilized to treat boundary conditions. MFM and NEM employ the strategy of prior artificial-selected element node layout which is also largely dependent on the empiricism. IGAM has some pitfalls like WFEM. In a word, all those above or other methods are short of the parameter-resolution level (RL) with a clear mathematical sense that can be easily used to fully alter total element node number and locate element node because they do not have a simple, clear and solid mathematical basis. However, MEM has such a simple, clear and rigorous mathematical basis that brings about the parameter RL to freely adjust total node number and locate nodes within the element. Hence, it can be said that WFEM, MFM, NEM, IGAM etc are the intermediate products in the transition of the traditional FEM from the monoresolution (discretized model) to the multiresolution (integrated model) and MEM consolidates all these irrational MRA approaches.

## 7. Conclusion and Prospective

A new multiresolution element method that has both high power of resolution and strong flexibility of analysis clarity is introduced into the field of numerical analysis. The method possesses such prominent features as follows:

1. A new split-full node notion is presented and a novel technique is proposed to construct a simple and clear basic full node shape function for a triangular plate-bending element, which unveils the secrets behind assembling artificially of node-related items in global matrix formation by the conventional FEM.
2. A mathematical basis for the MRA framework, that is the displacement subspace sequence, is constituted out of the scaled and shifted version of the basic full node shape function, which brings about the rational MRA concept together with the RL.
3. The traditional 3-node triangular plate-bending element method is a monoresolution one and also a special case of the proposed. An element of superior analysis clarity surely contains more nodes when compared with that of the inferior.
4. The RL adjusting for the multiresolution triangular plate-bending element model is laid on the rigorous mathematical basis while the meshing or remeshing for the monoresolution is based on the empiricism. The proposed element method can consolidate all corresponding irrational MRA approaches. Thus, the accuracy of a plane-bending analysis is replaced by the clarity, the irrational MRA by the rational, the mesh by the RL that is the discretized model by the integrated.
5. A quite new concept is introduced into the FEM that the structural analysis clarity is actually determined by the RL-the density of node uniform distribution, not by the mesh.
6. With advent of the new finite element method [17,18,19], the rational MRA will find a wide application in numerical solution of engineering problems in a real sense.

The upcoming work will be focused on the treatment of interface between multiresolution elements of different RL. The interface may be extended to the bridging domain in which a transitional element could be used just as PS images of different RL. The transitional element could also be constructed by the technique of scaling and shifting of the basic full node shape function to virtual or real nodes.

## References


[1] Zienkiewicz,O.C. and Taylor,R.L. The Finite Element Method. seventh ed., Butterworth-Heihemann, London. (2013)

[2] Xiang, J.W., Chen, X.F., He, Y.M and He, Z.J. The construction of plane elastomechanics and Mindlin plate elements of B-spline wavelet on the interval. Finite Elements in Analysis and Design, **42**: 1269-1280 (2006)

[3] He, Z.J., Chen, X.F., and Li, B. Theory and engineering application of wavelet finite element method, Science Press, Beijing (2006)

[4] Yu, Y., Lin, Q. Y. and Yang, C. A 3D shell-like approach using element-free Galerkin method for analysis of thin and thick plate structures. Acta Mechanica Sinica, **29**: 85-98 (2013)

[5] Liu, H.S. and Fu, M.W. Adaptive reproducing kernel particle method using gradient indicator for elasto-plastic deformation. Engineering Analysis with Boundary Elements, **37**: 280–292 (2013)

[6] Sukumar, N., Moran, B. and Belytschko, T. The natural elements method in solid mechanics. International Journal of Numerical Methods in Engineering.**43**: 839-887 (1998)

[7] Sukumar, N., Moran, B. and Semenov, A.Y. Natural neighbor Galerkin methods, International Journal of Numerical Methods in Engineering. **50**: 1-27(2001)

[8] H. Lian, P. Kerfriden, S.P.A. Bordas , Shape optimization directly from CAD: An isogeometric boundary element approach using T-splines, Computer Methods in Applied Mechanics and. Engineering. **317**: 1–41(2017).

[9] T.J.R.HughesJ.A.CottrellY.Bazilevs**,** Isogeometric analysis: CAD, finite elements, NURBS, exact geometry and mesh refinement. Computer Methods in Applied Mechanics and. Engineering. **194(**39-41): 4135–4195(2005) .

[10] Artioli, E., Auricchio, F., Veiga, L.B. Second-order accurate integration algorithms for von-Mises plasticity within nonlinear kinematic hardening mechanism, Computer Methods in Applied Mechanics and Engineering, **196**: 1827-1846 (2007)

[11] Feng, X.T. and Yang, C.X. Genetic evolution of nonlinear material constitutive models, Computer Methods in Applied Mechanics and Engineering. **190**: 5957-5973(2001)

[12] Jäger, P., Steinmann, P. and Kuhl, E. Modeling three-dimensional crack propagation—A comparison of crack path tracking strategies, International Journal of Numerical Methods in Engineering, **66**: 911-948 (2006)

[13] Fagerström, M. and Larsson, R. Theory and numerics for finite deformation fracture modelling using strong discontinuities, International Journal of Numerical Methods in Engineering. **76**: 1328-1352(2006)

[14] Luccioni, B.M., Ambrosini, R.D. and Danesi, R.F. Analysis of building collapse under blast loads. Engineering Structure, **26**: 63-71 (2004)

[15] Wang, Z.Q., Lu, Y. and Hao, H, Numerical investigation of effects of water saturation on blast wave propagation in soil mass. ASCE- Engineering Mechanics, **130**: 551-561 (2004)

[16] Long, Y.Q., Cen, S. and Long, Z.F. Advanced Finite Element Method in Structural Engineering. Springer-Verlag GmbH: Berlin, Heidelberg; Tsinghua University Press: Beijing, 2009

[17] Xia, Y. M., Liu, Y. X., Chen, S.L.and Tan, G. A rectangular shell element formulation with a

new multi- resolution analysis. Acta Mechanica Solida Sinca. **27(6)**:612-625(2014)
[18] Xia, Y. M. A multiresolution finite element method based on a new quadrilateral plate element. Journal of Coupled Systems and Multiscale Dynamics. **2(2)**:52-61 (2014)
[19] Xia, Y. M., Chen, S.L. A hexahedron element formulation with a new multi-resolution analysis. Science China (Physics, Astronomy and Mechanics), **58(1)**: 014601-10 (2015)